Department of Physics and Astronomy
University of Heidelberg

Bachelor Thesis in Physics
submitted by

Andrea Bergschneider

born in Oberviechtach (Germany)

2010

Studies of Lithium Atoms in a Magneto-Optical Trap

This Bachelor Thesis has been carried out by Andrea Bergschneider at the
Kirchhoff Institute in Heidelberg
under the supervision of
Prof. Dr. Markus K. Oberthaler

Abstract

This thesis describes the preparation for and the realization of a magneto-optical trap for cooling fermionic lithium. It allows further steps towards a sodium-lithium experiment for investigating polaron physics.

After a basic description of the principles of laser cooling and trapping, the optical requirements for lithium are introduced. The experimental realization of the optical setup is then presented, focusing on dual wavelength fiber coupling of sodium and lithium light. In addition the static and dynamic properties of the laser locking system, realized with a frequency offset-lock, are explored, yielding a frequency ramptime of 0.9 ms for a 30 MHz-jump. Finally the trapping optimization and the characterization of the MOT are described and a brief introduction is given on the absorption imaging, being an important tool for further experiments.

Kurzfassung

In dieser Arbeit werden die Vorbereitung und Umsetzung einer magneto-optischen Falle zum Kühlen von fermionischem Lithium beschrieben. Dadurch werden weitere Schritte in Richtung eines Natrium-Lithium Experiment ermöglicht, das zur Erforschung von Polaron-Physik dienen soll.

Nach einer grundlegenden Beschreibung der Kühl- und Einfang-Prinzipien mit Lasern, werden die optischen Anforderungen für Lithium vorgestellt. Anschließend wird die experimentelle Umsetzung des optischen Aufbaus dargestellt, wobei ein besonderes Augenmerk auf das Koppeln von Strahlen mit zwei verschiedenen Wellenlängen, denen von Natrium und Lithium, in dieselbe Faser gelegt wird. Außerdem werden die statischen und dynamischen Eigenschaften des Laser Lock-Systems via Frequenzabstandslock, untersucht, wobei bei einen Sprung von 30 MHz eine Regelzeit von 0.9 ms erreicht wurde. Zuletzt werden die Einfangoptimierung und Charakterisierung der MOT beschrieben und eine kurze Einführung in die Methode der Absorptionsabbildung gegeben, die ein wichtiges Instrument für weitere Experimente darstellt.

Contents

Chapter 1

Introduction

A large part of matter in our environment consists of solids. The examination concerning their existence, structure and physical properties is essential for our understanding of nature.

Many phenomena in solid state physics are of quantum mechanical nature of which many are not yet fully understood on a fundamental level. Here quantum statistics plays a dominant role. The most obvious example are electrons in a metal, forming a degenerate Fermi gas at room temperature.

Based on quantum mechanics and statistics, first theoretical approaches considering crystal structures of solids were tackled with next-neighbor interactions, leading to the well-known Hubbard model. It describes electrons moving in a periodic potenial of an ionic lattice explaining especially conduction properties of metals. However, most solids cannot be described by this simple model, but the necessary, more extensive models are hard to solve even numerically. Furthermore experimental verification of the theoretical models is hampered due to thermal effects or lattice imperfections.

One way to circumvent this problem is to mimic a considered physical system by another quantum system that allows experimental investigation, acting as a "quantum simulator" according to a suggestion of R. P. Feynman in 1982 [1]. Ultracold quantum gases are an interesting candidate, as they provide a good control of temperature, atom number, internal state or coherence as well as the interaction between the atoms. The resulting synthetic systems allow precise measurements which can be described by theoretical models.

A breakthrough on the way to quantum simulation with ultracold gases was the realization of Bose-Einstein condensation in 1995 [2, 3] and a degenerate Fermi gas [4] in 1999. By using optical lattices acting as micropotentials on atoms, artificial crystals can be constructed that provide an opportunity to investigate predictions of the Hubbard model. The experimental access to the potential depth allows the observation of the superfluid-Mott-insulator quantum phase transition [5, 6].

Apart from the potential shape, in ultracold quantum physics the interparticle interactions play an important role. In the limit of vanishing kinetic energy applicable for ultracold quantum gases, the interaction can be characterized by a single parameter, the s-wave scattering length. By applying an external field, its sign and absolute value can be modified by means of Feshbach resonance [7]. For fermions

suitable Feshbach resonances exist only in spin-mixture systems due to the Pauli exclusion principle [8]. The tunable scattering length offers the opportunity to go to regimes of strong interaction. For large repulsive interaction, bosonic molecules can be formed made out of spin-up spin-down fermions being superfluid, whereas for large attractive interaction between fermions, Cooper pairing can be simulated, which had been predicted by Bardeen, Cooper and Schrieffer in order to explain the solid state phenomenon of type I superconduction in certain metals [9].

Except for the simulation of solids, what new insights can be gained by the examination of fermionic spin-mixture systems? Imbalanced spin mixtures show exciting features due to the existence of a partially polarized phase. In contrast to a superfluid, where spin pairing occurs, in this phase few fermions in one spin state act like impurities in a sea of fermions with the other spin state. The many-body interplay of a moving impurity in a sea of fermions with strong interaction can be described by a quasiparticle, the Fermi polaron [10]. As the interaction between sea and moving impurity effects a drag force, an effective mass can be associated to the quasiparticle [11].

In solid state physics, however, polarons follow from the interaction of single electrons with a bath of bosonic phonons. In order to simulate this situation, a Bose-Fermi mixture can be used in which few fermionic particles play the role of the electrons. They are immersed in a sea of bosons forming a Bose-Einstein condensate. The so-called Bogoliubov excitations [12] of the BEC mimic the phonons in this system and are created by the presence of the impurities. The polaron properties can then be analysed with regard on the interaction strength between impurity and boson or on the properties of the excitations [13]. Although simulating a phenomenon usually appearing in metals, an underlying lattice structure does not play a role at least for the Fröhlich polaron, as neither the distribution of the impurities nor of the phonons form a lattice.

In our experiment, the Bose-Einstein condensate is provided by ^{23}Na-atoms, whereas ^{6}Li acts as the impurity. This requires combined trapping and cooling mechanisms of the two species. Using Feshbach resonances the coupling between fermion and bosonic bath can be influenced and examined. One can also think of moving the ^{6}Li-atoms through the BEC in order to gather further information on the polarons, e. g. their effective mass in dependence of the coupling. All this might offer a possibility to simulate solid state physics in order to gain some new insight into not yet well understood phenomena, e. g. high-temperature superconductivity.

Outline of the thesis

This thesis reports on the preparation and characterization of a magneto-optical trap of fermionic lithium atoms, that provide the impurities in a sea of sodium atoms for future polaron experiments.

Chapter 2 introduces the principles of laser cooling and magneto-optical trapping. Their application on ^{6}Li and the necessary optical transition frequencies for the cooling scheme will be discussed in the second part of this chapter. The experimental

realization of the required optical setup will be dealt with in chapter 3. In addition, a special focus is put on the basics and experimental techniques of dual wavelength fiber coupling of sodium and lithium light which provides the possibility to assure an overlap of the magneto-optical traps of both species. In chapter 4 the frequency offset-lock is presented by first giving a brief overview on its basic working principles. A characterization concerning static and dynamic properties illustrates the possibilities of changing the laser frequency of the main laser while being still beat-locked on a spectroscopy-locked master laser. Chapter 5 shows the results of the foregoing preparations. With the fluorescence method, the atom number is determined and loss processes can be characterized by considering loading and decay measurements. The second part introduces the absorption imaging being the method of choice for further experiments as it provides spatial resolution. The necessary experimental timing is presented with special regard on the frequency jump properties of the offset-lock, facilitating future measurements on lithium which is important at high magnetic fields, where relevant Feshbach resonances are situated.

Chapter 2

Basic Requirements for Laser Cooling and Trapping of ^{6}Li

In the following, the principles of cooling atoms in a magneto-optical trap will be presented, with a special focus on ^{6}Li. First, fundamentals of optical cooling and magneto-optical trapping will be introduced briefly. The second part will present the experimental setup with a focus on the required optical system to prepare and cool the lithium atoms.

2.1 Cooling Atoms with Light

Slowing atoms with light forces is a common method to cool atoms to temperatures of submillikelvin corresponding to a velocity of a few meters per second. This can be done by near-resonant photon-scattering resulting in the so-called *radiation pressure force*.

In the following the description of a two-level atom will be used to derive the principle mechanisms of laser cooling. This is in most cases sufficient as the laser light that is used to drive one transition is off-resonant to all the other existing transitions, as can be seen in figure 2.1 (a). The two-level description breaks down when atoms can decay into a lower ground state where a further optical excitation is off-resonant, which will be discussed in section 2.2.

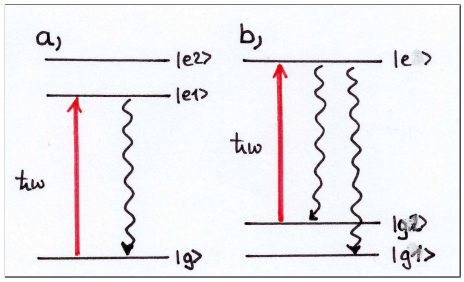

Figure 2.1: (a) Resonant excitation to only one transition. Here the two-level description is valid. (b) Two-level description breaks down, as the resonant excitation leads to a subsequent loss of the atom into an off-resonant ground state.

2.1.1 Radiation Pressure Force

When an atom absorbs a resonant photon, it gains the photon energy $\hbar\omega$ and gets a recoil $\Delta p = \hbar k$ due to the momentum of the absorbed photon. This change in momentum can be expressed as a force acting on the atom. Subsequently, the excited atom emits a photon with the momentum $\hbar k$. This spontaneous emission process takes place in a random direction after a certain lifetime τ and the mean recoil momentum of the spontaneous emission vanishes. Thus, a directed flux of photons, i. e. a light beam, causes a directed force on the atom.

The radiation pressure force acting on an atom due to absorption and subsequent emission of a photon is

$$F_{\text{scat}} = \frac{\Delta p}{\Delta t} = \hbar k \gamma_{\text{scat}} = \hbar k \Gamma \rho_{ee}. \tag{2.1}$$

It depends on the momentum of the scattered photon $\hbar k$ and on the scattering rate γ_{scat}, which is the decay rate $\Gamma = 1/\tau$ times the population probability of the excited state ρ_{ee}. The latter is dependent on the intensity I and the detuning δ with respect to the optical transition. With a higher saturation parameter $s_0 = I/I_s$, which denotes the ratio of the intensity to the saturation intensity I_s, as well as a lower detuning $\delta = \omega - \omega_0$, the excitation probability raises, reaching a maximum value of 1/2. This results in a maximal scattering force of $F_{\text{scat}} = \hbar k \Gamma/2$. Solving the optical Bloch equation, we obtain [14]

$$F_{\text{scat}} = \frac{\hbar k \Gamma}{2} \frac{s_0}{1 + s_0 + (2\delta/\Gamma)^2}\,. \tag{2.2}$$

The detuning δ can be caused not only by detuning the laser frequency, but also by a motion of the atom or an external magnetic field, resulting in a Doppler or Zeeman shift, respectively, as explained in the following.

The velocity dependent frequency shift due to an atom's motion is called the *Doppler shift*. In the atom's frame a counterpropagating photon is seen with blue detuned frequency whereas a copropagating photon is red detuned. In the lab frame, the detuning with respect to the transition frequency is $\delta_{\text{D}} = -\vec{k}\vec{v}$ for an atom moving with velocity $\vec{v}$ and a transition with the wave number $\vec{k}$. A velocity of 600 m/s of lithium atoms with $\lambda = 671\,\text{nm}$ as transition wavelength thus results in a detuning of about $1\,\text{GHz} = 200\,\Gamma$. So, scattering on counterpropagating atoms in order to dissipate kinetic energy requires red detuning with respect to the transition frequency at rest [15]. But the consequent deceleration gets the atoms avidly out of resonance. To avoid this, one can make use of applying a magnetic field.

The energy level shift due to an external magnetic field B is called the *Zeeman effect* and is affected by a coupling between magnetic moment $\mu \neq 0$ and magnetic field. It results in an energy shift $\Delta E = -\vec{\mu} \cdot \vec{B} = -m_j g_j \mu_{\text{B}} B$ weightened with the magnetic quantum number m_j, which can take the values $m_j = -j, -j+1, ..., +j$ with j being the total angular momentum of the electron. This leads to a discrete lift of the degeneracy of the magnetic substates. The Landé factor g_j denotes

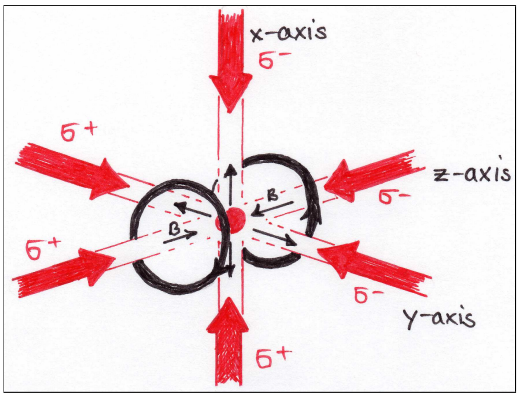

Figure 2.2: 3-dimensional schematic of a magneto-optical trap. Six laser beams (red) are radiated to the center of the trap, being perpenticular to each other. Anti-Helmholtz coils provide the inhomogenous magnetic field (black).

the dependency on the coupling of the atom's angular momenta[1] [15]. An optical transition from $|j, m_j\rangle$ to $|j', m_j'\rangle$ obtains therefore a detuning of

$$\delta_{\mathrm{Z}} = -\frac{1}{\hbar}(m_j' g_j' - m_j g_j)\mu_{\mathrm{B}} B = -\frac{\Delta\mu' B}{\hbar}. \tag{2.3}$$

These two effects are used to slow down moving atoms by light force in a *Zeeman slower*. For a deceleration of atoms with a counterpropagating laser beam, the resonance condition has to be valid at any place of the atom's trajectory. Thus a spatially varying magnetic field is applied that compensates the Doppler shift of the moving atom, such that photon absorption leading to a loss of kinetic energy is possible over a long distance [16, 17].

2.1.2 Magneto-Optical Trap

The same techniques as described above, can be used to cool and trap atoms in a magneto-optical trap (MOT). In contrast to the one beam in the Zeeman slower, we use six beams, one from each direction, as shown in figure 2.2. Their light frequency is red shifted with respect to the transition with δ_l and affects a dissipating force F_{scat} on the atoms against their momentum direction. But in addition, the atoms have to be trapped to be able to observe and manipulate them. This can be achieved by altering the strength of the scattering force by detuning. For the implementation of a spatially varying detuning of the atomic transition, an inhomogenous magnetic field is applied by an anti-Helmholtz configuration, having zero magnetic field in the trap center, as depicted in figure 2.2.

A one-dimensional schematic of the MOT is shown in figure 2.3. The linear magnetic field $B(z) = B'z$ leads to a Zeeman splitting of the upper magnetic

[1] A consideration of the total angular momentum, denoted by $F = I + j$ considering also the nuclear momentum I can be done in a similar way by using the Landé factor of the total angular momentum g_F.

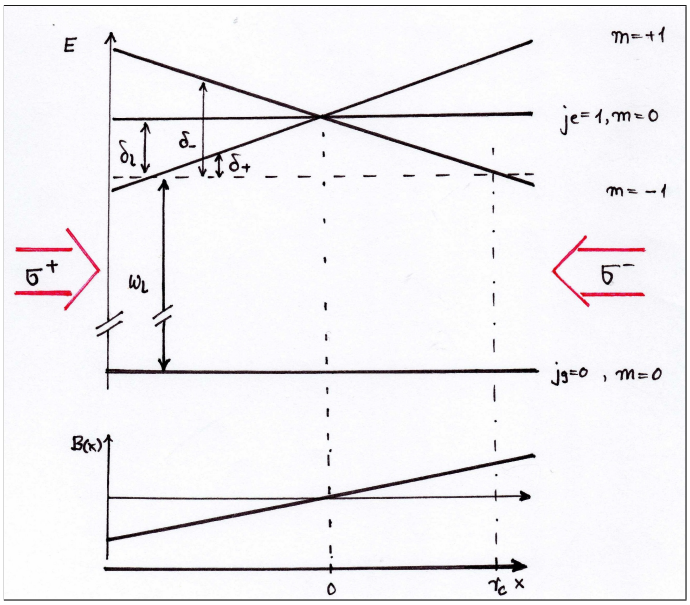

Figure 2.3: Simplified scheme of a magneto-optical trap. A linear magnetic field is applied, splitting the magnetic sublevels of $|j_e = 1\rangle$ states. Laser light with a detuning of $\delta_l < 0$ is radiated from two sides with circular polarization exerting a force on the atoms near resonance. Here, δ_+ and δ_- are the detunings for atoms at rest.

substates m. In addition, σ^+-polarized light is radiated from the left side and σ^--polarized from the right side[2] . Hence, only optical transitions from $|j, m\rangle = |0, 0\rangle$ to $|1, \pm 1\rangle$ are possible due to selection rules. The light frequency is red detuned with respect to the transition and consequently, atoms moving outwards absorb more light due to Zeeman and Doppler shift. The resulting recoil towards the trap center leads to a confinement of the atoms [18].

MOT Forces and Capture Properties

The radiative force on the atoms in the MOT can be expressed by

$$\vec{F} = \vec{F}_+ + \vec{F}_- = \frac{\hbar \vec{k} \Gamma}{2} \left(\frac{s_0}{1 + s_0 + (2\delta_+/\Gamma)^2} - \frac{s_0}{1 + s_0 + (2\delta_-/\Gamma)^2} \right), \tag{2.4}$$

with the total detuning

$$\delta_\pm = \delta_l \mp \vec{k}\vec{v} \pm \frac{\Delta \mu' B}{\hbar}, \tag{2.5}$$

which is a sum of the laser detuning $\delta_l < 0$, the Doppler and the Zeeman shift, depending on the velocity and the magnetic field, respectively.

[2]The circular polarization direction is defined with respect to the same quantization axes, which is the z-axis in this case.

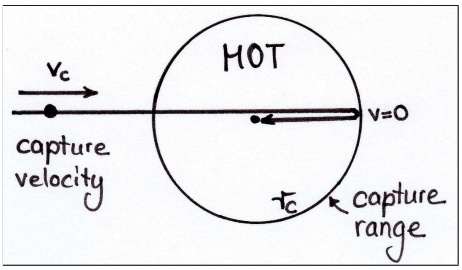

Figure 2.4: Capture process of an atom in a MOT. The atom moving with v_c towards the MOT crosses one time and is stopped at the capture range r_c, before being confined in the trap center.

Considering only cold atoms nearby the trap center, the force can be expanded in a Taylor series around $B = 0$ and $v = 0$, which leads to

$$\vec{F} = -\beta\vec{v} - \kappa\vec{r}. \tag{2.6}$$

The first term denotes the friction force dissipating energy from the system with β being the friction coefficient. The second part is a restoring force responsible for the trapping with κ being the spring constant. Consequently, near the trap center the atoms' motion can be described by a damped harmonic oscillator [18].

A difficulty appears regarding atoms with $\delta_D \approx \delta_l$. Then the expansion leading to equation 2.6 is no longer valid as the velocity and thus the Doppler detuning δ_D is large. This is especially the case for the atom capture process. So, characteristic quantities to know about are the capture properties of the trap, both *capture range* and *capture velocity*.

The capture range r_c can be determined as the maximal radial position where slow atoms can stay without leaving the trap. This is roughly the case if $\Delta E_{\delta_l} = \Delta E_{\delta_{\text{Zeeman}}}$ and thus

$$r_c = \frac{\hbar|\delta_l|}{\Delta\mu' B'}\,. \tag{2.7}$$

With the capture range, a simplified calculation of the so-called capture velocity v_c, can be done. It is the maximal velocity of an atom that can be decelerated to $v = 0$ before reaching the capture range after crossing the complete magneto-optical trap one time, as shown in figure 2.4. Based on the assumption of a constant deceleration of the atom via light forces inside the r_c of the MOT, we yield

$$v_c = \sqrt{\frac{2\pi\hbar^2\,\Gamma\,\delta_l}{\lambda_l\, m\,\Delta\mu'\,B'}} \tag{2.8}$$

with m the mass of the particle and λ_l the wavelength of the laser light.

To raise v_c, the detuning δ_l has to be enlarged as then atoms with higher Doppler shifts are resonant and can thus be decelerated. This can be done both by detuning the laser δ_l or changing the magnetic field gradient B' and permits to raise the

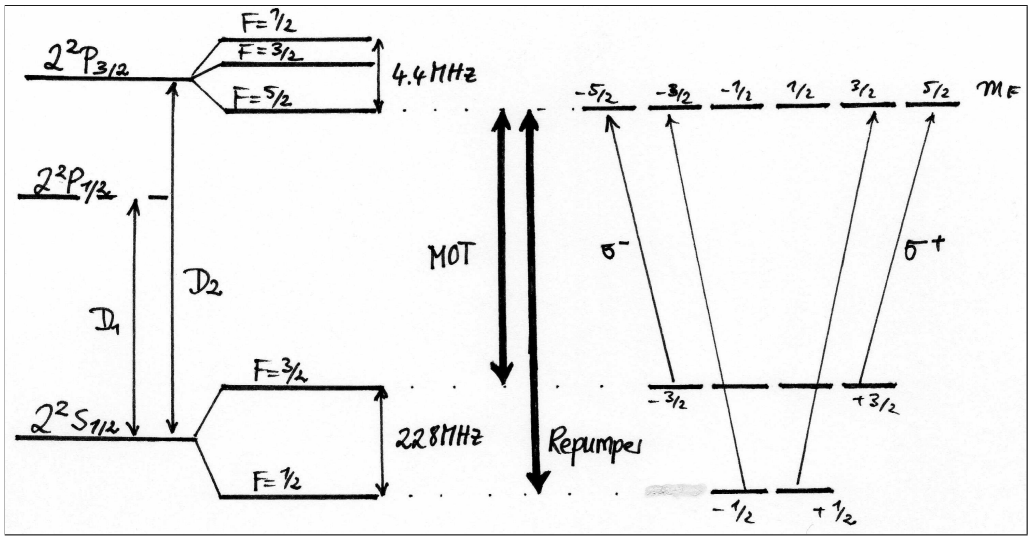

Figure 2.5: Level scheme of ^{6}Li. Due to I-j-coupling the levels are split up, denoted by F. With the help of the MOT and the repumper light, a cycling transition for the cooling process is assured. Furthermore, the circular light drives the outermost transitions of the atom.

trapping efficiency, which is one of the primary goals. By precooling with a Zeeman slower, the fraction of atoms with a velocity smaller than v_c is raised and the trapping efficiency can be improved [18, 19].

2.2 Level Scheme of ^{6}Li

The ^{6}Li-isotope consists of three protons, three neutrons and three electrons and is thus a fermion. This is important for further experiments, but has no relevance for the magneto-optical trapping. However, there is a differency in required laser frequency to the bosonic ^{7}Li in the order of MHz.

All alkali atoms have an optical transition in the visible or near-infrared wavelength regime, the so-called *D-Line*. For lithium, it is at about 671 nm. Considering the level scheme 2.5, we see that the D-Line consists actually of two main lines. This can be explained by finestructure splitting, caused by the coupling of the electron spin $\vec{s}$ with the angular momentum $\vec{l}$ to the total electron angular momentum $\vec{j} = \vec{l} + \vec{s}$ and is on the order of some GHz for ^{6}Li. Taking into account also the nuclear spin $\vec{I}$, that couples with the total electron angular momentum $\vec{j}$ to $\vec{F} = \vec{I} + \vec{j}$, we get a further level splitting on the order of MHz, called *hyperfine splitting*. The different energy scales are due to the difference of three orders of magnitude between magnetic moment of the nucleus μ_N and the Bohr magneton μ_B. [20]

The hyperfine splitting between the two substates of $2^2S_{1/2}$ is 228.2 MHz, whereas for the three hyperfine levels of $2^2P_{3/2}$ we get 4.4 MHz. This splitting is smaller than the natural linewidth of the D_2-Line being 5.87 MHz. Thus the three levels cannot

be resolved. [21].

Every F-level consists of $2F + 1$ degenerate magnetic substates, denoted as m_F. Due to the selection rules, absorption of circular polarized light results in a magnetic quantum number change of $\Delta m_F = \pm 1$. But the emission process has no prefered polarization. Thus, after a few cycles, most of the atoms will be in the *cycling transition* $m_F = \pm 3/2 \rightarrow \pm 5/2$.

For the MOT-transition, we use $F = 3/2 \rightarrow F'$, but as the upper levels F' overlap within their width, there is a finite transition probability to levels in which the atoms decay to $F = 1/2$, and are thus not trapped any more. Therefore, a second optical frequency is used, driving $F = 1/2 \rightarrow F'$. This light is called *repumper* and pumps the lost atoms back into the cycling transition $F = 3/2 \rightarrow F'$, as shown in figure 2.5.

In conclusion, a magneto-optical trap uses the scattering force of light in order to cool atoms. For ^{6}Li-atoms a MOT and a repumper frequency are required, in order to prevent atoms from leaving the cycling transition, as in this system the simple two-level description is not valid.

Chapter 3

Laser System for Cooling ^{6}Li

In this chapter, the experimental generation of the necessary laser light frequencies and the MOT-setup for cooling ^{6}Li will be presented. In addition, the optical setup will be explained, with special focus on the requirements and techniques of dual wavelength fiber coupling of lithium and sodium light.

3.1 Optical Setup

The MOT beams and the slower beam will be derived from one single laser. Therefore, it has to be split up into several beams, which get different frequency shifts via acousto-optic modulators. In our experiment the MOT and slower beam intensities need to be a few times higher than the saturation intensity, in order to avoid a high sensitivity on the laser power. Thus about 200 mW are required, met by a so-called *Tapered Amplifier*, which is in the following denoted as TA.

3.1.1 Laser Frequency Schematics and MOT Setup

For laser cooling experiments, stable light frequencies in the order of the linewidth are essential. This means a stabilization of about 400 THz on the level of a few MHz. In our experiment, a grating stabilized diode laser, in the following denoted as master laser, is locked on the cross-over peak[1] of lithium via Doppler-free absorption spectroscopy [17]. A part of the master laser beam is overlapped with a part of the TA beam in order to stabilize the TA on the resulting beat $\Delta\nu = \nu_{\mathrm{TA}} - \nu_{\mathrm{Master}}$. For the MOT phase, we have $\Delta\nu = -65\,\mathrm{MHz}$, as can be seen in the frequency schematic in figure 3.1.

In order to keep the atoms available for the laser cooling process, MOT and repumper light, as well as slower and slower repumper light are necessary, as it has been deduced in section 2.2. The frequency difference between MOT and repumper beam is 228 MHz, and their detuning with respect to the respective transition frequency is $\delta_l = -30\,\mathrm{MHz}$, as proposed by [19]. For the slower beam, MOT and repumper have to be both red detuned by -300 MHz, which in combination with the slower parameters determines the fraction of decelerated atoms [16].

[1] The cross-over is a peak appearing in the middle of the $F = 1/2 \rightarrow F'$ and $F = 3/2 \rightarrow F'$ transitions.

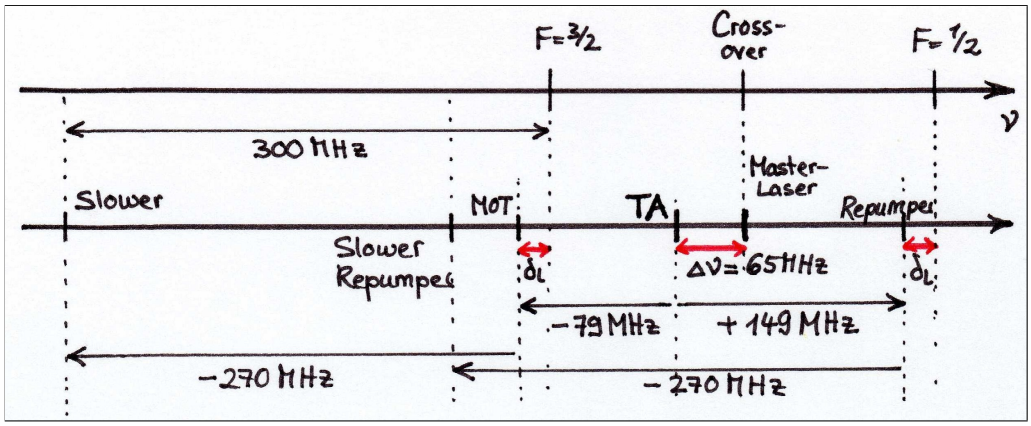

Figure 3.1: Frequency scheme of the laser setup. The m aster laser is stabilized on the cross-over peak, providing beat-locking of the TA with $\Delta\nu = -65\,\mathrm{MHz}$.

The frequency combination can be achieved by shifting the TA frequency by $-79\,\mathrm{MHz}$ for the MOT light and by $+149\,\mathrm{MHz}$ for the repumper light. For the slower light, the MOT and the repumper light will be shifted further by $-270\,\mathrm{MHz}$. This is done with one single AOM.

As we aim on investigating a sodium-lithium atom mixture, a further requirement is the spatial overlap of sodium and lithium MOT position, which can be achieved by guiding the beams through the same optical fibres. This is advantageous not only regarding the limited space on the experimental optical table, but it also provides a combined adjustment of lithium and sodium beams for the magneto-optical trap. The only disadvantage is the challenge to accomplish high coupling efficiencies for both beams.

The anti-Helmholtz configuration for the magnetic field of the MOT provides a pancake shaped magnetic potential. In the direction of the weaker confinement, retro-reflected MOT-beams are irradiated. In the following, they are denoted as the x- and y-beams, and have a higher intensity than the ones in the direction of stronger magnetic confinement. The resulting roughly round shape of the MOT allows an effective transfer into the magnetic trap. For the axial direction of the MOT, two counterpropagating beams with independently adjustable intensities, denoted as z-beams, are implemented. By imbalancing the z-beam intensities, the center of the MOTs can be shifted in z-direction for sodium as well as for lithium in an independent way. This offers the possibility to separate the sodium and lithium MOTs, avoiding inter-species light assisted collisions of sodium and lithium, which leads to a two-body loss process [22].

3.1.2 Experimental Realization of the Optical Setup

In order to fulfill all the requirements mentioned above, the optical setup, depicted in figure 3.2, has been established. The main output beam of the tapered amplifier is first scaled down by a tunable 2:1 telescope, as its output waist is too large to be

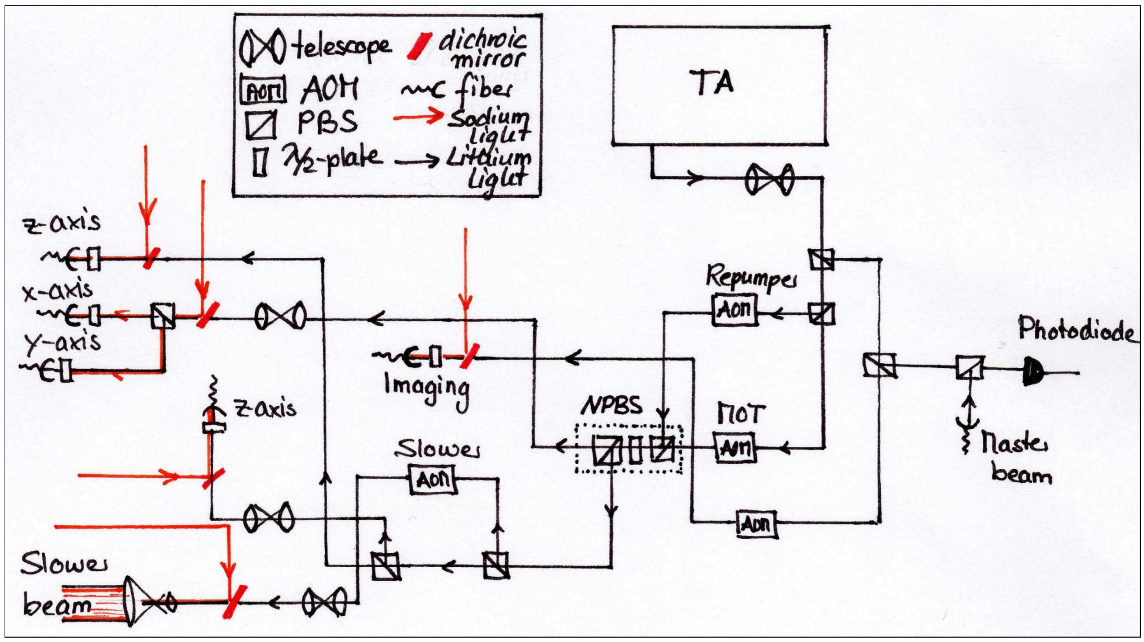

Figure 3.2: Lithium laser setup. The TA beam is subdivided in imaging, MOT and repumper beam, shifted independently via AOM. Then the MOT and repumper beam are overlapped and subdivided again, providing MOT and slower light. For overlapping with the sodium light, dichroic mirrors are used. Only the relevant optical elements are depicted.

coupled into the optical fibers efficiently (see section 3.2). Then, it is splitted into imaging, MOT and repump beam.

All three beams are frequency shifted by acousto-optic modulators (AOM) with a soundwave propagating in horizontal direction through the crystal and acting like a grating onto the light. For a collimated beam incidenting at the Bragg angle, the diffraction gets most efficient. But, as the soundwave is very narrow in vertical direction, the beam has to be focused by a cylinder lens for sufficient overlap. Behind the AOM, the beam is collimated again and the unwanted diffraction orders are dumped by an iris.

The Imaging beam is directly coupled into an optical fiber, whereas the MOT and repumper beams are overlapped before. The combination of two polarizing beam splitters with a half wave plate in between mimics a non-polarizing beam splitter, yielding 2 beams, each containing the same MOT-repumper power ratio. One branch provides the light for the x- and y-beams, the other for the two z-beams and the slower light.

The overlap of the lithium beam with the sodium beam is achieved by using dichroic mirrors transmitting the lithium light very well at a special angle, and at the same time reflecting the sodium light efficiently. Being overlapped this way, the two beams can be coupled into the same optical fiber. For better fiber coupling efficiency of the lithium beam, a tunable 4:5 telescope is set in front of each dichroic mirror to

adapt waist and divergence of the beam, as described in Section 3.2.3.

After passing the polarization maintaining fibers, the polarization is cleaned by a polarizing beamsplitter cube. The light gets then circularly polarized by a quarter-wave plate, before being expanded by a telescope to a beam waist of 1 cm. Having different wavelengths, the wave plate cannot transform the sodium and lithium polarization equally well, but as a compromise we use zero order retarders that are at 633 nm.

3.2 Dual Wavelength Fiber Coupling

Our goal is to couple sodium and lithium light into the same optical fiber efficiently for both wavelengths. This requires a tuning of different degrees of freedom of both beams as e. g. its waist and divergence.

3.2.1 Gaussian Beam

When a laser beam is focused, the common ray optic concept breaks down, as one cannot achieve an infinitesimally small focus due to the diffraction limit. Instead, the Helmholtz equation, resulting from wave optics, gives a valid description. Considering typical laser beam parameters as used in the lab, the paraxial approximation can be applied, yielding the *gaussian beam* as a solution which is characterized by its radial gaussian intensity shape

$$I(\rho, z) \propto \exp\left[-\frac{2\rho^2}{w^2(z)}\right] . \tag{3.1}$$

Its beam width is defined as $w(z) = w_0\sqrt{1 + (z/z_R)^2}$, with the finite waist w_0 at the focus and the Rayleigh range z_R, which is defined by the distance from the beam focus to the position, where $w(z) = \sqrt{2}w_0$. For $z \gg z_R$, a beam divergence $\theta = w_0/z_R$ can be defined.

When focusing a collimated gaussian beam at a wavelength of λ with a lens having a focal length f, we get the relation

$$w_0' = \frac{\lambda f}{\pi w_0} \approx \theta_0 f \tag{3.2}$$

for the waist w_0' behind the lens. It strongly depends on the chosen focal length and on the waist of the incoming beam w_0, which is meaningful for the fiber coupling technique [23].

3.2.2 Principles of Fiber Coupling

An optical fiber allows to guide light over large distances. Conceptionally, it consists of two layers of optically transparent material with slightly different refraction indices.

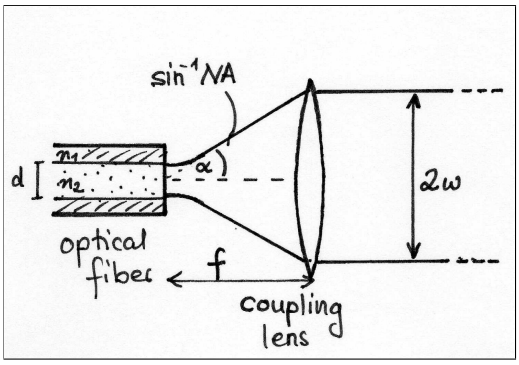

Figure 3.3: Fiber coupling scheme. The collimated beam is focused on the fiber end with a coupling lens yielding a minimal waist in the order of the fiber core.

The inner core has a refraction index of n_2 and a diameter of d, whereas the enveloping cladding has $n_1 < n_2$. By an adaption of the core diameter and the refractive index difference, the fiber can be made *single mode* for a certain wavelength, as the higher modes have larger spatial extensions and are thus damped strongly [23].

As we aim on guiding sodium and lithium light together through an optical fiber, it has to be single mode for both wavelengths. Therefore, a single mode fiber specified for lithium is used[2], which is also single-mode for 589 nm, as $\lambda_{\mathrm{Li}} < \sqrt{2}\lambda_{\mathrm{Na}}$, with $\sqrt{2}\lambda_{\mathrm{Na}}$ being the spatial extension of the next higher transverse mode TEM_{01}.

When exiting the optical fiber, the guided laser beam spreads with an angle of 2α, as depicted in figure 3.3. This is usually expressed by the *numerical aperture* $NA = n \sin\alpha$, where n is the surrounding medium's refractive index and equal to 1 in our case. To collimate the light, an outcoupling lens is needed, providing a waist that given by

$$w = 0.82 \cdot f \cdot NA\,. \tag{3.3}$$

with 0.82 being a numerical factor resulting from the definitions of the beam waist and the numerical aperture. As the optical path can be reversed, this relation is also valid for the incoupling.

3.2.3 Simultaneous Coupling of Sodium and Lithium Light

For efficient fiber coupling, as can be seen in figure 3.3, we need basically two degrees of freedom, which are the distance between incoupling lens and fiber end to match the numerical aperture and the size of the incoming beam waist. For sodium, the beam waist is adapted by a telescope and the incoupling lens distance such that the transit efficiency gets maximal.

For the lithium beam it is thus not possible to adjust the incoupling lens anymore. However, we can get two degrees of freedom by using two tunable telescopes. A 2:1

[2]Thorlabs PM-S630-HP specified for $630 - 780$ nm with a mode field diameter of $4.2(5)\,\mu$m at 630 nm, a numerical aperture $NA = 0.12$ and a second mode cut-off at 580(40) nm. The fiber obtains PANDA stress rods for polarization maintaining.

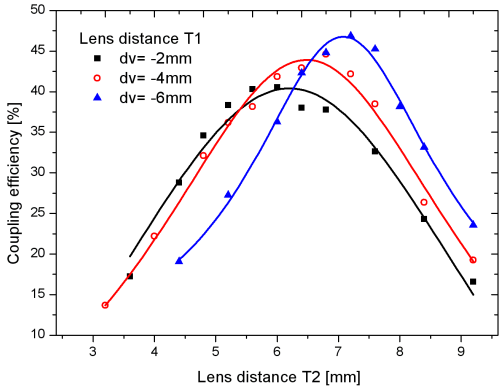

Figure 3.4: Coupling efficiency dependent on the settings of two telescopes. With decreasing lens distance of T1, the maxima get more pronounced and more critical. The lines are gauss fits to determine the optimal lens distance T2. For the sake of clarity only three representative front telescope settings are plotted.

telescope (T1) is set right behind the TA and the second telescope with the focal length ratio of 4:5 (T2) is set in front of each dichroic mirror, as depicted in figure 3.2. With the combined tuning of the two telescopes the waist and the divergence of the laser beam can be adjusted. The optimization has been done on the x- and y-beam fibers, being the most critical due to the light power requirement, with the result to be seen in figure 3.4. There, we mapped out the fiber coupling efficiency in dependence of the rear telescope for different front telescope settings. Note that for higher maximal efficiency, the tuning gets also more critical. With this technique an efficiency of about 50% has been achieved for all 4 MOT fibers providing the necessary light power on the experimental optical table.

Chapter 4

Frequency Offset-Lock

This chapter deals with the static and dynamic frequency stabilization of the Tapered Amplifier wavelength via *frequency offset-locking*. In the first part, a short overview of the signal detection and locking method will be given, before characterizing the device for further implementation. We will focus on the beat frequency adjustment, as well as on dynamic aspects concerning the loop velocity.

4.1 Principles of Offset-Locking

As we cool lithium atoms with near-resonant light, it is suitable to lock the laser on an atomic transition line via Doppler-free spectroscopy. A required offset to the locking frequency can be arranged via an AOM, that shifts the light by a defined frequency. If a variable offset up to a range of GHz is needed, frequency shifting with AOM is not possible as both the diffraction angle and efficiency depend on the AOM frequency. But by using a second laser and stabilizing a resulting beat signal between the outputs of the two lasers with an *offset-lock*, the requirements can be fulfilled. We thus get a large tunability range of the laser frequency, which is required for absorption imaging on resonance at different magnetic fields, especially at $B \approx 1\,\mathrm{kG}$, where the relevant Feshbach resonances are located.

In our experiment, we use a grating stabilized diode laser with a linewidth of about 1 MHz and low power. It is locked on the a lithium atomic transition via Doppler-free spectroscopy. The frequency stabilization is done using a Lock-In in combination with a loop-amplifier [17]. The second laser, that provides the power for the experiment, is a tapered amplifier, which is locked on the diode laser (master) via offset-lock.

4.1.1 Creation of the Error Signal

A superposition of two laser beams with slightly different frequency leads to a beating with $\Delta\omega = \omega_2 - \omega_1$. This beating, in our case resulting from an overlap of the spectroscopy-locked master laser with ω_1 and the Tapered Amplifier with ω_2, is detected by a fast photodiode and mixed with a radio frequency ω_{VCO} from a voltage controlled oscillator (VCO), as to be seen in figure 4.1. The mixing yields difference and sum, latter of which is filtered out by a low-pass. A splitting and delay by τ_{delay}

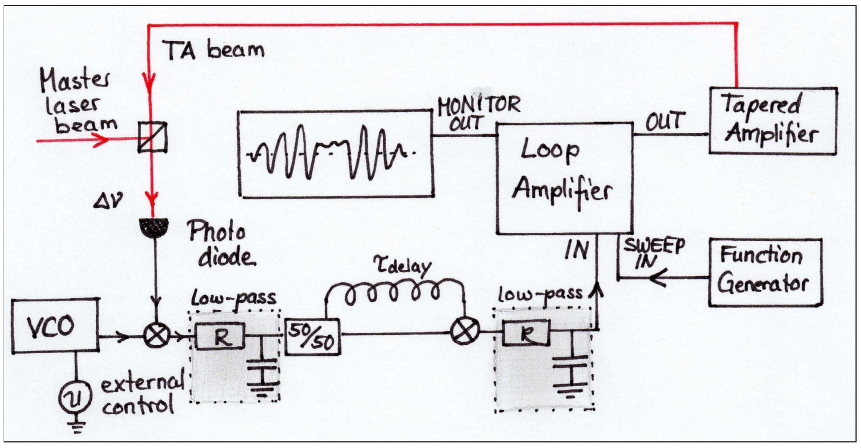

Figure 4.1: Locking and feedback scheme for the TA. The beat, resulting from an overlapped of master laser and TA is detected by a fast photodiode. Out of the beat, an error signal is created with the offset-lock electronics and fed into the loop-amplifier for the locking. It outputs a feedback signal for the TA.

of one of the signals provides a relative phase shift ϕ. Subsequently, they are mixed again and pass another low-pass filter leading to a dc signal given by [24]

$$\cos\phi = \cos((\Delta\omega - \omega_{\mathrm{VCO}})\tau_{\mathrm{delay}})\,. \tag{4.1}$$

Sweeping the TA frequency with a function generator results in a varying beat $\Delta\omega$ which then provides, according to equation 4.1, an error signal in form of a cosine, as to be seen in figure 4.2 (a). The zero-crossings of this cosine function are possible locking points. During the laser locking on one of the zero-crossings, a change in the radio frequency ω_{VCO} to a certain value yields a shift of the laser frequency as $\Delta\omega - \omega_{\mathrm{VCO}}$ is fixed by a loop-amplifier.

4.1.2 Locking and Feedback

The error signal, described in section 4.1.1, is fed into the loop amplifier, as figure 4.1 shows. For sweeping the TA laser frequency, a linear ramp is passed through the sweep input of the loop amplifier to the signal output. This is connected with the piezo of the TA, providing a possibility to tune the frequency of the TA by changing the laser cavity slightly. The sweep range and offset can be tuned with the loop-amplifier and with the monitor output, the error signal can be monitored on an oscilloscope. When the locking is active, it displays the difference between process value and the setpoint. For adjusting the speed of feedback control, the loop amplifier has proportional and integral controllers which are separately switchable and tunable. With the loop-amplifier output the piezo of the laser cavity is controlled.

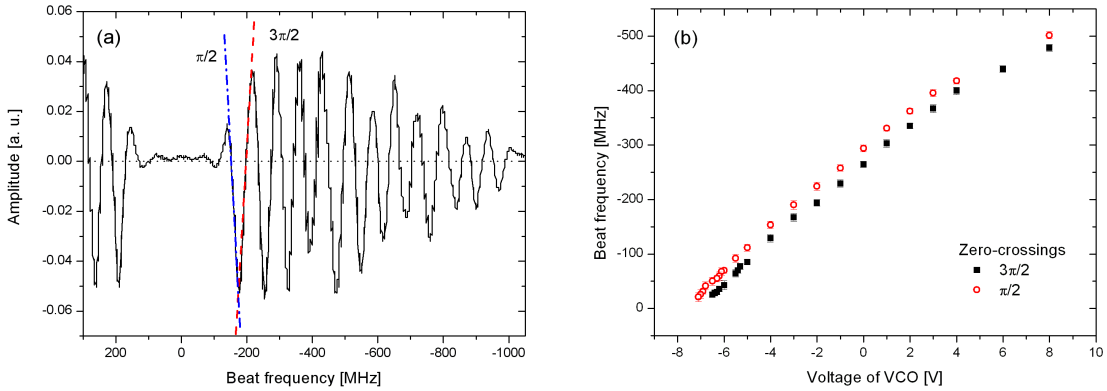

Figure 4.2: (a) The error signal provided by the offset-lock. In the right part of the signal, the TA-frequency is red detuned with respect to the master laser. The locking is performed on the first long positive slope near the zero-point. (b) The calibration curve, mapping the relation between VCO-voltage and beat frequency for two explicit slopes.

4.2 Static Characterization of the Offset-Lock

Our first interest is to map out the dependency of the beat signal $\Delta\nu$ on the VCO-voltage for different locking slopes of the error signal. We are only interested in a detuning of the TA, that is negative and can be shifted up to $\Delta\nu = -35\,\mathrm{MHz}$ with respect to the cross-over frequency. Thus we choose the two next zero-crossings to $\Delta\nu = 0$, as can be seen in figure 4.2 (a) where the $\pi/2$-slope (blue, dashed doted) is the first negative and the $3\pi/2$ (red, dashed) the first positive slope. We use 2.5 m long delay line, providing a zero-crossing distance of 38 MHz in beat frequency. In figure 4.2 (b), the dependency on the VCO-voltage is shown for the two slopes, yielding a maximal possible beat frequency of $-20\,\mathrm{MHz}$. As we want to assure a good stability and a high loop velocity of the locking for later shifting, we chose the $3\pi/2$-slope for further measurements, as it is the longer and steeper one.

4.3 Dynamical Properties of the Offset-Lock

For the absorption imaging at $B = 0$, the TA frequency has to be switched from a beating of $\Delta\nu = -65\,\mathrm{MHz}$ for the MOT-loading phase to $\Delta\nu = -35\,\mathrm{MHz}$, thus hitting the transition resonance. This requires a beat shift of 30 MHz in a short ramptime.

The range of a frequency jump is mainly limited by the distance of the zero-crossings in case of optimal loop control. The loop direction is given by the sign of the difference between process value and setpoint, as depicted in figure 4.3 (a). If the process value is larger than the setpoint, the loop amplifier e. g. diminish the output

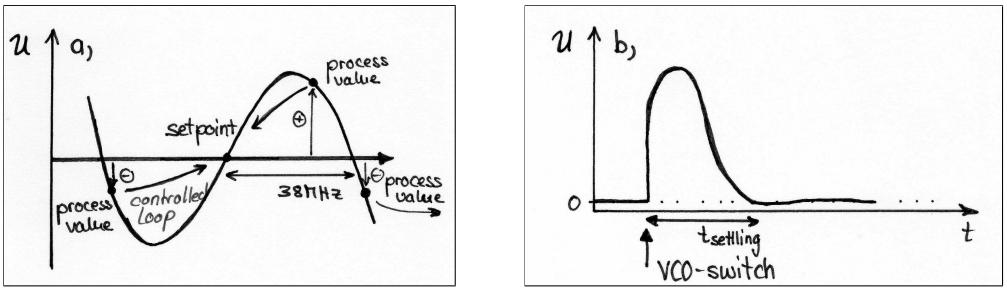

Figure 4.3: (a) Schematic of the loop control. The loop direction is dependent on the sign of the process value with respect to the setpoint. (b) Schematic of the step response of a VCO-voltage jump. The time until the process value is again equal to the setpoint is denoted as t_{settling}.

voltage in order to shift the laser frequency back to the setpoint. But if the frequency is further away than 38 MHz, the process value is negative, the loop-amplifier tries to shift the frequency towards the next zero-crossing and thus the laser is not locked any more. Consequently, with the used delay line it is only possible to perform jumps of about 30 MHz. For larger steps, the VCO voltage has to be ramped up gradually.

The loop velocity is given by the loop's integral control and the load i. e. the capacity of the piezo. In order to characterize the dynamics of the frequency shift, the overshoot caused by a voltage jump, a so-called step response, is examined, as can be seen in figure 4.3 (b). With that, we measured the dependence of the settling time on the integral time constant, which is adjustable by tunable resistors R and capacities C and obtain a minimal value of $t_{\text{settling}} = 0.9\,\text{ms}$, below which the lock is unstable. It has been assured that the settling time corresponds approximately to the time constant determined by the electronics, that is given by $\tau = RC$.

In summary, our offset-lock allows to switch the TA laser frequency from $\delta_l = -30\,\text{MHz}$ to $\delta_l = 0\,\text{MHz}$ with respect to the MOT transition in $t_{\text{ramp}} = 0.9\,\text{ms}$. The pure beat signal has a width of 2.5 MHz, measured by a spectrum analyser, corresponding to the convolution of the master and the TA linewidth, which is 1.8 MHz for both. Frequency shifts in the range of more than 0.5 GHz are not yet possible as the VCO range is not large enough. However, a switching between different VCOs with overlapping frequency ranges would offer the opportunity to ramp the TA to the required frequency for imaging of lithium at Feshbach resonances.

Chapter 5

Experimental Realization of the ^{6}Li-MOT

In the following chapter, two methods for quantitative measurements of the lithium MOT atom number are presented: the *fluorescence method*, providing a simple possibility of real time examination, and the *absorption imaging*, being the tool of choice especially for advanced measurements together with sodium.

5.1 Characterization of the MOT via Fluorescence

One very simple possibility to do quantitative measurements on the atom cloud in the magneto-optical trap is the *fluorescence method*. It allows measurements of the atom number and the dynamics of the MOT. However, it provides no information on density distributions.

5.1.1 Atom Number Measurements

The fluorescence method is based on the detection of scattered photons of the MOT. With an exact knowledge about the fraction of the detected light in comparison to the total emitted light, one gets information about the atom number.

Fluorescence light is emitted in random direction. Its total power is determined by the atom number N, their scattering rate γ_{scat} and the photon energy $\hbar\omega_0$. As the light passes through an uncoated glass cell, the transmitted light is diminished by a factor of $t^2 = (0.96)^2$. In addition, only light of a certain solid angle $\mathrm{d}\Omega$, which is 0.015 in our setup, can be detected. This angle is given by the lens which images the MOT on the photodiode. It converts the light into current, which can be read out by a resistor and depends on the light intensity. The device used in the following provides $\epsilon = 0.44\,\mathrm{A/W}$ for $\lambda = 671\,\mathrm{nm}$.

So, we obtain

$$N = \frac{U_{\mathrm{osci}}}{R_{\mathrm{osci}}} \cdot \frac{4\pi}{\hbar\omega_0\,\gamma_{\mathrm{scat}}\,\epsilon\,t^2\,\mathrm{d}\Omega} \tag{5.1}$$

for the atom number, where U_{osci} and R_{osci} are the signal voltage on the oscilloscope and its input impedance.

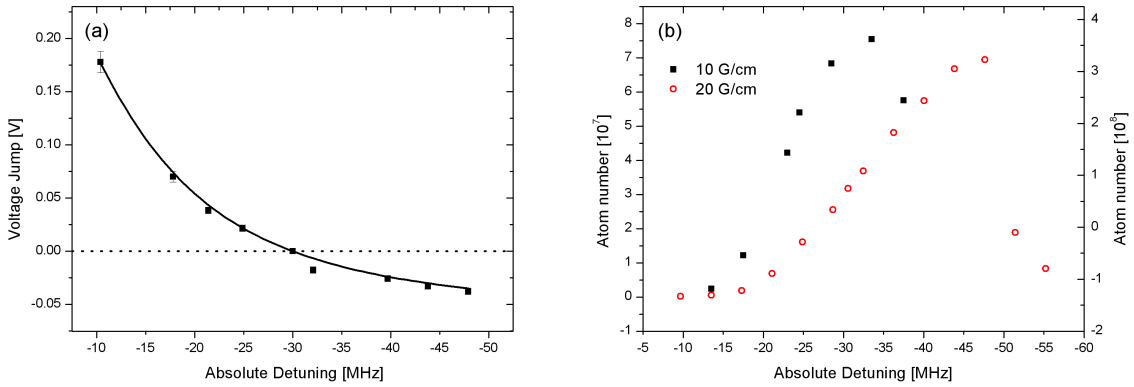

Figure 5.1: (a) Measurement of the detuning jump after MOT saturation. According to equation 5.2, a fit has been proceeded with the independent parameters s_{eff} and N (solid line). (b) Influence of the laser detuning on the MOT size. For a field gradient of 10 G/cm the maximal number of atoms trapped in the MOT is at $\delta_l = -5\Gamma$. For higher gradients, the value decreases.

In order to derive the atom number from the signal, we have to know the scattering rate γ_{scat} very well, as introduced in equation 2.2. The detuning of the MOT-beams is $\delta_l = -30\,\text{MHz}$ corresponding to -5Γ. In addition, we estimate the saturation parameter s_{eff} as the sum of all MOT-beam intensities over the saturation intensity $I_s = 2.54\,\text{mW/cm}^2$ and obtain $s_{\text{eff}} \approx 18$. Thus, the scattering rate is $\gamma_{\text{scat}} \approx 2.7 \times 10^6\,\text{atoms/s}$ and yields about $2.7 \times 10^6\,\text{atoms/mV}$ for the conversion of signal height to atom number. However, due to a presence of a spatially inhomogeneous magnetic field influencing the detuning, it is not clear whether the estimate is justified.

A possibility to examine the dependency of the scattering rate γ_{scat} on the detuning δ and the saturation parameter s_{eff} is to measure it as a function of the one parameter and fit the other. A possible Ansatz for experimental verification is to change the scattering rate γ_{scat} by a jump in TA detuning at a constant atom number N and measure the voltage jump ΔU_{PD}, affected by the changed scattering condition. With the help of our offset-lock, we are able to change the detuning in a time of 0.9 ms and the jumps can be done very precisely. The dependence of the photodiode voltage jump ΔU_{PD} on the detuning jump from $\delta = -30\,\text{MHz}$ to δ_f yields the saturation parameter s_0 and the atom number N as independent fit parameters. For $\delta_f > \delta$ the voltage jump is positive due to a suddenly higher scattering rate. The general relation can be assumed as

$$\Delta U_{\text{PD}} = N\,\hbar\omega_0\,\epsilon\,t^2\,\mathrm{d}\Omega\,\frac{\Gamma}{2}\left(\frac{s_{\text{eff}}}{1+s_{\text{eff}}+(2\delta_f/\Gamma)^2} - \frac{s_{\text{eff}}}{1+s_{\text{eff}}+(2\delta/\Gamma)^2}\right). \qquad (5.2)$$

A fit of the function 5.2 on the measurements with the free parameters N and s_{eff} can be seen in figure 5.1 (a) and yields an atom number of $N_{\text{fit}} = 1.6(1) \times 10^8$ and a

saturation parameter of $s_{\text{eff}} = 18(3)$. For the measurement we presumed that the detuning δ corresponds to the detuning of the TA, but actually the Doppler shift of the moving atoms and the Zeeman shift of the magnetic field have to be taken into account for the scattering rate. Moreover, the summation of the beam intensities is not clear. But further measurements, e. g. a detuning jump in absence of a magnetic field gradient, promise to gain more insight in the validity of the assumption.

Using the fitted s_{eff}, the simple fluorescence measuremement yields an atom number of $N_{\text{fm}} = 1.8(3) \times 10^8$ which is in agreement with N_{fit} within the error. From our simplified ansatz, we received $s_{\text{eff}} = 18(3)$ and derive a conversion factor of $2.7(4) \times 10^6\,\text{atoms/mV}$, which is only valid for $B' = 10\,\text{G/cm}$ with $\delta_l = -5\Gamma$ and will be used in the following.

5.1.2 MOT Optimization

With the tool of fluorescence imaging at hand, a primary goal for the further experiments is to optimize the atom number N and the loading rate of the captured atom cloud in the trap. The loading rate is determined as the initial slope of the loading signal. A good MOT, i. e. a large amount of cold atoms loaded in a short time, can be achieved by:

- a proper crossing of all the MOT beams at the magnetic field center, which has already been done for sodium.
- a light intensity of the MOT beams that is a few times the saturation intensity for each beam, in order to avoid a sensitivity of the atom number on light power fluctuations, and an additional power balancing between the different axes.
- a high flux of trappable atoms, which is mainly depending on the deceleration properties of the Zeeman slower and the amount of atoms provided by the atom source. [17]
- a proper circular polarization of the MOT-beams, as a wrong polarization would affect a light force pushing atoms out of the trap.
- an efficient repump process to pump atoms back into the *cycling transition*, which have been decayed into the wrong ground state. So, a sufficient intensity of the *repumper* beam with respect to the MOT-beam has to be assured. In our experiment the ratio of MOT-beam to repumper intensities is 2.5 .
- an optimized balance between laser detuning δ_l and magnetic field gradient B'. This last point has to be discussed a little bit more carefully.

The detuning δ_l determines the temperature of the atom cloud which should not be to high. The ratio of δ_l and B' sets the size of the cloud $r_c \propto \delta_l/B'$ and the critical velocity $v_c \propto \sqrt{\delta_l/B'}$ of the trappable atoms, deduced from equations 2.7

and 2.8. Fixing the detuning, a higher gradient of the magnetic field leads to a decreasing atom number, as the MOT size as well as the capture velocity decrease. In addition, we would expect also a decreasing loading rate as smaller v_c means a smaller flux of capturable atoms for the MOT loading, but this is not the case. In contrast, the loading rate increases for higher magnetic field gradient and saturates at about $B' = 15\,\mathrm{G/cm}$. This may be due to a disturbing influence of the small Zeeman slower field [16, 17], which decreases with higher MOT-field and raise the amount of trappable atoms. In our experiment, we fixed $B' = 10\,\mathrm{G/cm}$. Changing the laser detuning, the MOT size is maximal at about $\delta_l = -5\Gamma = -30\,\mathrm{MHz}$, as it can be seen in figure 5.1 (b). For lower δ_l and fixed B', the atoms get colder but the capture velocity and range decrease and hence the atom number and loading rate. For higher gradients, the optimum is also at a higher $|\delta_l|$, as depicted in figure 5.1 (b).

5.1.3 Loading and Lifetime Dynamics

The dynamics of the magneto-optical trap, i. e. the rate equation for the atom number N_{atoms}, is not only affected by the loading rate, denoted as L. There are also loss processes leading to a saturation of the loading curve and therefore to a limited atom number as well as a finite lifetime of the trapped cloud. The rate equation describing the dynamics is given by [25]

$$\frac{\mathrm{d}N}{\mathrm{d}t} = L - \frac{1}{\tau_{\mathrm{MOT}}}N - \beta\frac{N^2}{V} \tag{5.3}$$

and contains besides of the loading rate L two kinds of loss processes that are the *one-* and *two-body losses*. Three-body losses are not important in a magneto-optical trap as its density is not high enough by far.

The one-body processes, represented by the second term on the right hand side, are scattering processes with the background gas and the atoms arriving from the Zeeman-slower. The trap's lifetime τ_{MOT} is therefore not dependent on the atom number in the trap and the decay rate consists of $1/\tau_{\mathrm{MOT}} = 1/\tau_{\mathrm{decay}} + 1/\tau_{\mathrm{source}}$, where τ_{decay} and τ_{source} are the contributions of background-scattering processes and the scattering with the untrappable atoms from the atomic beam. The one-body loss processes result in an exponential growth and decay for loading and lifetime characteristics.

The two-body losses, in contrast, depend on the atom density $\rho = N/V$ as they are due to scattering processes where two trapped atoms are involved. A pair of atoms in the ground state can be described by the $2^2\mathrm{S}_{1/2}$+$2^2\mathrm{S}_{1/2}$ molecular potential being very smooth. With an excitation of one of the atoms, the potential transfers to $2^2\mathrm{S}_{1/2}$+$2^2\mathrm{P}_{3/2}$. Subsequently, the two atoms move towards each other reducing the binding energy. From there on, two different processes can occur:

Either, the excited atom can emit one photon with lower energy and get back to the ground state. The energy difference between absorbed and emitted photon is transformed into kinetic energy leading to an escape of the atoms. This process

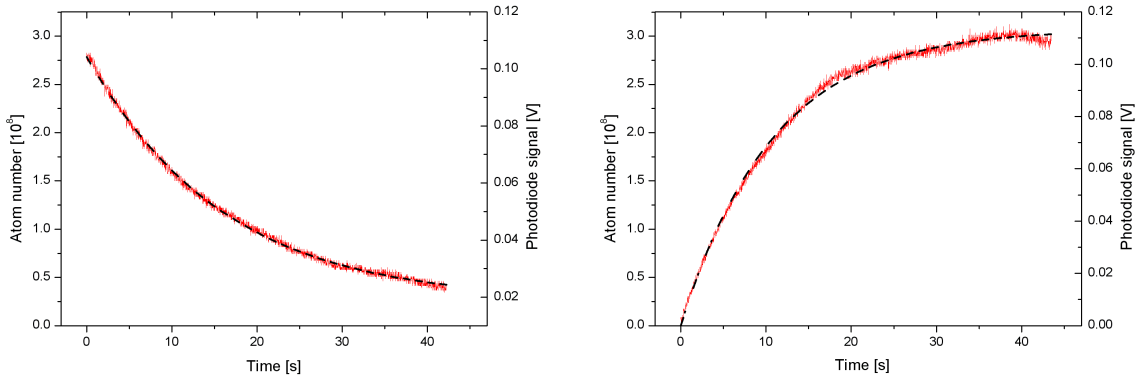

Figure 5.2: Loading and unloading curve of the magneto-optical trap. For the loading curve an exponential growth function is fitted (black, dashed). For the decay data, the function 5.4 has been fitted adding a constant offset.

is called *radiative escape*; or if the molecular potential of $2^2S_{1/2}+2^2P_{3/2}$ crosses the one of $2^2S_{1/2}+2^2P_{1/2}$ potential, the molecule can change the potential branch. That results in one atom in the ground state and one in $2^2P_{1/2}$, therefore called *fine-structure changing collision*.

The two-body losses are denoted as *light assisted collisions*. Their rate thus depend on the intensity of the MOT light and they are characterized by the decay rate coefficient β [18].

The loading and lifetime dynamics are measured via fluorescence. For the decay measurement, the slower light as well as the atomic beam have been interrupted. A solution of the differential equation with $L = 0$ and $N_{\text{decay}}(0) = N_0$ yields :

$$N_{\text{decay}}(t) = N_0 \frac{e^{-t/\tau}}{1 + N_0 \tau \beta' t (1 - e^{-t/\tau})}, \tag{5.4}$$

with $\beta' = \beta/\bar{V}$ and $\bar{V}$ being the average volume for an isotrope gaussian density distribution of the cloud. As fit parameter we get the lifetime $\tau_{\text{decay}} = 16.5(2)\,\text{s}$ and the modified decay rate coefficient $\beta' = 0.003\,/\text{s}$. The total atom number for $t = 0$ is $N_{\text{total}} = 2.8 \times 10^8$, as can be seen in figure 5.2. Comparing the contributions of the two loss terms, the two-body term is suppressed by a factor of 200 due to a low density of the atom cloud and could as well have been neglected.

Consequently, it is sufficient to fit the loading curve considering only one-body losses. There, we obtain a total atom number at saturation of $N_0 = 3.1(5) \times 10^8$ and a lifetime of $\tau_{\text{load}} = 10.9(1)\,\text{s}$. The latter is smaller compared to the decay process as during the loading, atoms from the slower beam collide with the captured atoms and thus induce losses. Furthermore, we obtain a loading rate of $L = 2.8(4) \times 10^7\,\text{atoms/s}$.

The signal offset due to scattered MOT light is about 3 mV. However, we obtain an offset of about 19 mV for the decay curve from the fit routine. This corresponds

to about 4.3×10^7 atoms staying in the MOT although no atoms are captured from the Zeeman-slower beam. Hence, this suggests having a background MOT, i. e. there is a background gas of lithium in the glass cell which can be loaded in the MOT by the MOT-beams without being decelerated by the Zeeman slower before.

The fluorescence method provided a possibility for optimizing and examinating the magneto-optical trap. The final atom number in the atomic cloud is about 3×10^8 whereas more than half of them are loaded in 10 s with a magnetic field gradient of 20 G/cm. Furthermore, two-body losses in the atomic cloud are not important due to the low density.

5.2 Absorption Imaging

For further experiments, it is not sufficient to detect only a signal proportional to fluorescence. In order to be able to examine the dynamic behavior of the lithium atoms, e. g. as being an impurity in a bosonic bath, spatial resolution of the atoms' distribution is essential, which can be done by *absorption imaging*. In our case a frequency shift of the TA is required, provided by the offset-lock, such that the imaging light is in resonance with the atoms in the cloud.

5.2.1 Imaging Setup and Sequence

Absorption imaging is based on resonant light absorption of the trapped cloud. A collimated imaging beam is directed on the MOT and detected with a CCD camera. The resulting shadow image of the cloud is focused on the camera, resulting in a projected density distribution image. The imaging beam waist is larger than the size of the atom cloud and the intensity has to be low, leading to an absorption which is proportional to the atom number.

Our measurement sequence for absorption imaging of the MOT, depicted in figure 5.3, consists of a MOT-loading phase and an imaging phase. During the MOT-phase, the MOT beams as well as the slower, the atomic beam and the magnet gradient field are powered. For the imaging, only the repumper light of the MOT beams is still on and the resonant imaging beam is pulsed with a duration of 80 μs [17]. In order to assure several absorption processes of the imaged atoms, the powering of the repumper light is necessary to pump the atoms back into the cycling transition. As the TA frequency has to be shifted between MOT and imaging phase with the help of the offset-lock, a time lag of at least 1 ms is performed, denoted as time-of-flight.

5.2.2 Detuning measurement

In order to find the exact resonance frequency of the atom cloud, the absorption dependent on the imaging frequency has been measured. As the frequency shift via AOM is the same for imaging as for the MOT light, we expect a required shift of

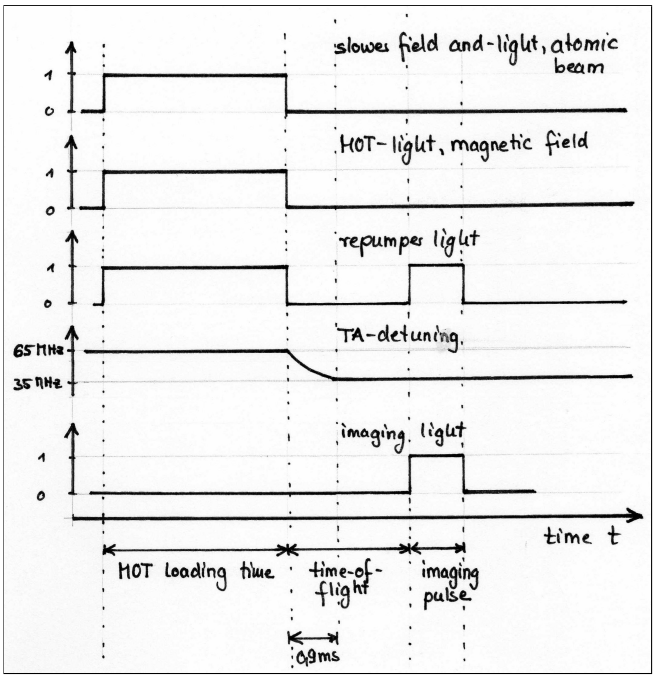

Figure 5.3: Experimental timing for absorption imaging. After the MOT loading and a time-of-flight, the MOT is imaged. During the time-of-flight, the TA frequency is shifted by the offset-lock, which requires 0.9 ms.

about the MOT-detuning δ_l for the imaging phase. The measurement is depicted in figure 5.4, fitted by a Lorentz function. For the peak position we obtain a beat frequency of 36.0(4) MHz[1], which corresponds to our expectation within the linewidth (see figure 3.1). Slight variations can be due to an unprecise set of the frequency shift of the AOM or of the locking points, but this will not be a problem.

The peak width obtained from the fit routine is $\Delta\omega = 2\pi \cdot 8.49(17)$ MHz exceeding the natural linewidth of the transition. This is due to the temperature of the atom cloud resulting in a Doppler broadening. A rough estimate yields a temperature in the range of a few millikelvin, which exceeds the expectation of about 500 μK [22] as the imaging heats up the atoms. With the density distribution of the atom cloud, a more precise temperature measurement can be accomplished, but as the lithium atoms will end up in a sample of a hundred times more sodium atoms thermalizing with them, their temperature is not of any relevance.

In conclusion, the absorption imaging provides a spatial resolution of the atoms' density distribution, but it is a destructive method. Thus, it is necessary to design an experimental sequence providing a high repetation rate of the measurement. Therefore, the TA frequency has to be shifted in each sequence. In addition, a rough estimate of the MOT temperature yield a few millikelvin for a imaging duration of 80 μs which may be too long.

[1]This corresponds to a VCO-voltage of $-7.03(1)$ V for optimal resonance during imaging at $B = 0$.

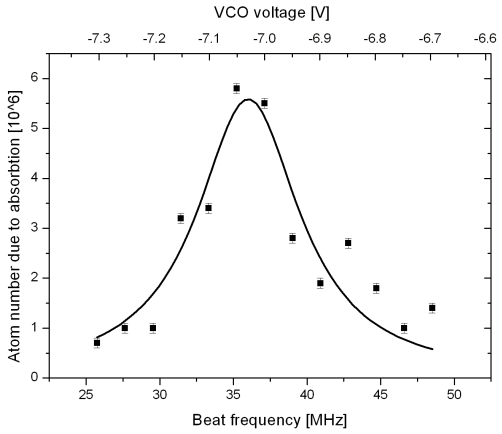

Figure 5.4: Absorption signal dependent on imaging frequency. Therefore, the TA frequency shift with respect to the spectroscopy cross-over frequency has been varied, probing the resonance of the atomic cloud.

With the help of the thermal density distribution the atom number can be measured more precisely than with the fluorescence method. Our final MOT consists of 4×10^8 atoms [17], which is sufficient for further experiments. The imaging method offers the possibility to do also measurements in a combined atomic sample leading towards polaron physics.

Chapter 6

Conclusion and Perspectives

This thesis has presented the preparation for and investigation of a magneto-optical trap for fermionic Lithium as the first cooling step, leading towards the realization of a Bose-Fermi mixture experiment.

The basis for further experiments was built up by the realization of a laser cooling system for ^{6}Li providing laser light to decelerate and confine atoms in a magneto-optical trap. In particular, a high coupling efficiency of Lithium light through optical fibers, already adjusted for the Sodium MOT, has been accomplished. After some optimization the resulting MOT now consists of 3×10^8 atoms, measured by fluorescence. In addition, the optimal red detuning of the MOT light for a magnetic field gradient of 10 G/cm has been measured to be $-5\,\Gamma$. Via real-time fluorescence imaging, the MOT dynamics have been characterized, yielding a loading rate of 2.7×10^7 atoms/s and loss processes only due to one-body losses with a lifetime of $\tau = 16.5$ s.

Moreover, the necessary optical preparations for absorption imaging have been done. For this imaging process, it is necessary to shift the frequency of the laser to the transition resonance. This is possible for arbitrary magnetic fields, performed by the frequency offset-lock. It has been characterized with regard to its locking stability, tuning range and dynamical properties, yielding a minimal ramptime of 0.9 ms due to fast operation of the loop-amplifier with possible frequency jumps of 30 MHz. This is sufficient for switching from MOT loading to imaging at zero magnetic field with a minimal time-of-flight of about 1 ms, and for a gradual change of the main laser frequency for higher magnetic fields.

The next step will be to load sodium and lithium together in the MOT and transfer them into the magnetic trap, where further cooling techniques can be applied. As fermionic lithium can not be cooled evaporatively because scattering and thus thermalization at that low temperatures is not possible for identic fermions, sodium acts as the scattering partner for sympathetic cooling.

In order to be independent of a magnetic field, the combined cloud will then be transfered into an optical dipole trap. This offers the possibility to apply tunable magnetic fields in the range of up to 1200 G for exploring inter- and intra-species Feshbach resonances of sodium and lithium. They are an important tool in order to adjust the interaction strengths between the atoms in an almost arbitrary way. So, it is possible to examine interactions between sodium and lithium atoms under

different conditions. Furthermore, fermionic ^{23}Na-^{6}Li molecules can be formed by a ramping over Feshbach resonances with the prospect of producing a molecular degenerate Fermi gas.

With an additional species selective dipole trap in form of a standing wave, the lithium atoms can be independently addressed and moved through the sodium sample with different interparticle interaction strengths adjusted by Feshbach resonances. Dependent on the interaction between the BEC particles one can think of locally probing the superfluidity of the sodium BEC. In addition Fröhlich polarons can be mimicked by coupling of the impurity and the Bogoliubov excitations of the BEC. Dependent on the inter- and intra-species scattering lengths their properties can be examined. In order to measure their effective mass a dragging of the impurities through the BEC or an oscillation in the standing wave potential well can be taken into account. This provides new insight in polaron physics and might be one step further towards understanding solid state effects like superconduction type II.

Appendix A

Constants and Lithium Properties

Quantity		Value	Unit
Planck constant	h	$6.62606876(52) \times 10^{-34}$	Js
	$\hbar$	$1.054571596(82) \times 10^{-34}$	Js
Speed of light	c	2.99792458×10^{8}	m/s
Boltzman constant	k_B	$1.3806503(24) \times 10^{-23}$	J/K
Bohr magneton	μ_B	$9.27400949(80) \times 10^{-24}$	J/T

^{6}Li data and D2 line properties [21]

Quantity		Value	Unit
Mass	m	$9.9883414 \times 10^{-27}$	kg
Wavelength	λ	670.977338	nm
Frequency	ω_0	$2\pi \times 446.799677$	THz
Natural linewidth	Γ	$2\pi \times 5.8724$	MHz
Lifetime	τ	27.102	ns
Saturation intensity	I_{sat}	2.54	mW/cm^2

Bibliography

[1] R.P. Feynman. Simulating physics with computers. *International journal of theoretical physics*, 21(6):467–488, 1982.

[2] K.B. Davis, M.O. Mewes, M.R. Andrews, N.J. Van Druten, D.S. Durfee, D.M. Kurn, and W. Ketterle. Bose-Einstein condensation in a gas of sodium atoms. *Physical Review Letters*, 75(22):3969–3973, 1995.

[3] M.H. Anderson, J.R. Ensher, M.R. Matthews, C.E. Wieman, and E.A. Cornell. Observation of Bose-Einstein condensation in a dilute atomic vapor. *Science*, 269(5221):198, 1995.

[4] B. DeMarco and D.S. Jin. Onset of Fermi degeneracy in a trapped atomic gas. *Science*, 285(5434):1703, 1999.

[5] M. Greiner, O. Mandel, T. Esslinger, T.W. Hänsch, and I. Bloch. Quantum phase transition from a superfluid to a Mott insulator in a gas of ultracold atoms. *Nature*, 415(6867):39–44, 2002.

[6] R. Jördens, N. Strohmaier, K. Günter, H. Moritz, and T. Esslinger. A Mott insulator of fermionic atoms in an optical lattice. *Nature*, 455(7210):204–207, 2008.

[7] S. Inouye, M.R. Andrews, J. Stenger, H.J. Miesner, D.M. Stamper-Kurn, and W. Ketterle. Observation of Feshbach resonances in a Bose–Einstein condensate. *Nature*, 392(6672):151–154, 1998.

[8] K.M. O'Hara, S.L. Hemmer, S.R. Granade, M.E. Gehm, J.E. Thomas, V. Venturi, E. Tiesinga, and C.J. Williams. Measurement of the zero crossing in a Feshbach resonance of fermionic ^{6}Li. *Physical Review A*, 66(4):41401, 2002.

[9] J. Bardeen, L.N. Cooper, and J.R. Schrieffer. Theory of superconductivity. *Physical Review*, 108(5):1175–1204, 1957.

[10] A. Schirotzek, C.H. Wu, A. Sommer, and M.W. Zwierlein. Observation of Fermi polarons in a tunable Fermi liquid of ultracold atoms. *Physical review letters*, 102(23):230402, 2009.

[11] S. Nascimbene, N. Navon, KJ Jiang, L. Tarruell, M. Teichmann, J. Mckeever, F. Chevy, and C. Salomon. Collective oscillations of an imbalanced Fermi gas: axial compression modes and polaron effective mass. *Physical review letters*, 103(17):170402, 2009.

[12] N.N. Bogoliubov. *J. Phys. (USSR)*, 11(23), 1947.

[13] J. Tempere, W. Casteels, M.K. Oberthaler, S. Knoop, E. Timmermans, and J.T. Devreese. Feynman path-integral treatment of the BEC-impurity polaron. *Physical Review B*, 80(18):184504, 2009.

[14] C.C. Tannoudji, J. Dupont-Roc, and G. Grynberg. *Atom-photon interactions*. WILEY, 1998.

[15] W. Demtröder. *Experimentalphysik 3: Atome, Moleküle und Festkörper*. Springer, 2005.

[16] J. Krieger. Zeeman-Slower und Experimentsteuerung für das NaLi-Experiment. 2008.

[17] M. Neidig. A Frequency Stabilised Diode Laser for Exploring the Properties of a Lithium MOT. 2010.

[18] H.J. Metcalf and P. van der Straten. *Laser Cooling and Trapping*. Springer, 2002.

[19] V.V. Volchkov. Cold Lithium Atoms for Future Polaron Experiments. 2009.

[20] I.H. Hertel and C.P. Schulz. *Atom-, Molekul- und Optische Physik*. Springer Verlag, 2008.

[21] M.E. Gehm. Properties of ^{6}Li. *The current version of the document is available at http://www. phy. duke. edu/research/photon/qoptics/techdocs*, 58, 2003.

[22] Z. Hadzibabic. *Studies of a quantum degenerate fermionic lithium gas*. PhD thesis, 2003.

[23] B.E.A. Saleh and M.C. Teich. *Fundamentals of Photonics*. WILEY, 2007.

[24] B.M. Huber. Towards Realization of a Polaron Experiment. 2009.

[25] A. Cable, M. Prentiss, and NP Bigelow. Observations of sodium atoms in a magnetic molasses trap loaded by a continuous uncooled source. *Optics letters*, 15(9):507–509, 1990.

Danksagung

An dieser Stelle soll allen gedankt werden, die mich während der Zeit meiner Bachelorarbeit begleitet und unterstützt haben.

- Besonders bedanken möchte ich mich bei Prof. Markus K. Oberthaler, der mich in seiner Arbeitsgruppe aufgenommen und mir diese Arbeit ermöglicht hat. Sein Vertrauen in meine Kompetenz, seine ansteckende Begeisterung für Physik und seine fachlichen Anregungen haben mich enorm motiviert und die Zeit im Labor sehr spannend werden lassen.
- Außerdem möchte ich Prof. Selim Jochim für die Begutachtung dieser Arbeit danken.
- Mein ganz besonderer Dank gilt den Mitgliedern des NaLi-Teams, für die tolle Arbeitsatmosphäre, die gute Zusammenarbeit und all die lustigen Momente. Sie haben die Zeit der Bachelorarbeit zu einer ganz besonderen in meinem Studium werden lassen. Im einzelnen bedanke ich mich bei:
  - Steven Knoop, unserem holländischen Postdoc, für das Korrekturlesen dieser Arbeit - trotz Fußball ;). Er fand außerdem immer Zeit, mir über meine eigentliche Arbeit hinaus die größeren Zusammenhänge in unserem Experiment nahe zu bringen und war auch immer für spontane Gruppen-Grillabende bei sich zu Hause zu begeistern.
  - Tobias Schuster, der die Betreuung meiner Bachelorarbeit übernommen hat. Ich danke ihn für seine Geduld, seinen unverbesserlichen Optimismus und seine ehrliche Art. Ohne ihn wäre der Aufbau einer Lithium-MOT innerhalb von 8 Wochen nicht möglich gewesen. Außerdem hat er nicht nur die ersten Versionen dieser Arbeit kritisch Korrektur gelesen, sondern auch immer für genug Nervennahrung (Doppelkekse und Kaffee) und Spaß (Canon) während der Arbeit gesorgt.
  - Jens Appmeier, der auch in der letzten Schreibphase seiner Dissertation immer noch Zeit für meine Belange und Lust auf meine selbstgebackenen Kuchen hatte.
  - Raphael Scelle für seine unkomplizierte Art und das geduldige Ertragen der Lithium-Messungen, während derer das Voranschreiten seiner Arbeit oft blockiert war.
  - Arno Trautmann, für seine Unterstützung bei diversen LaTeX-Problemen. Ihm habe ich es zu verdanken, auf die spannende Physik ultrakalter Quantengase aufmerksam geworden zu sein.

  - Bernhard Huber, einem ehemaligen NaLi. Er hat während seiner Diplomarbeit 2009 den Offset-Lock gebaut und getestet und mir hilfreiche Tipps diesbezüglich gegeben.
  - meinem Mitstreiter Mathias Neidig, dem zweiten Bachelor-Studenten im Team für die tolle Zusammenarbeit und die hilfreichen Diskussionen. Ohne seinen Einsatz wäre die Lithium-MOT ebensowenig möglich gewesen.

- Weiterhin möchte ich der gesamten Matterwave-Gruppe danken für die tolle Atmosphäre und den Spaß im und außerhalb des Labors.

- Mein Dank gilt auch Jürgen Schölles und Alexander Leonhard für das Ausleihen diverser elektronischer Geräte und ihre Hilfsbereitschaft bei so manchen technischen Herausforderungen. Außerdem danke ich auch Herrn Spiegel und der Feinmechanik-Werkstatt für ihre technische Unterstützung.

- Zu guter Letzt möchte ich meinen engsten Freunden und meiner Familie danken. Sie haben mich während meines bisherigen Studiums und insbesondere während der Bachelorarbeit unterstützt und mir immer Rückhalt gegeben.

Erklärung

Ich versichere, dass ich diese Arbeit selbstständig verfasst und keine anderen als die angegebenen Quellen und Hilfsmittel benutzt habe.

Heidelberg, den 06.07.2010,